Sciencexpress Reports

Chiral nanophotonic waveguide interface based on spin-orbit interaction of light

Jan Petersen, Jürgen Volz,* Arno Rauschenbeutel*

Vienna Center for Quantum Science and Technology, TU Wien–Atominstitut, Stadionallee 2, 1020 Vienna, Austria.

*Corresponding author. E-mail: jvolz@ati.ac.at (J.V.); arno.rauschenbeutel@ati.ac.at (A.R.)

Controlling the flow of light with nanophotonic waveguides has the potential of transforming integrated information processing. Due to the strong transverse confinement of the guided photons, their internal spin and their orbital angular momentum get coupled. Using this spin-orbit interaction of light, we break the mirror symmetry of the scattering of light by a gold nanoparticle on the surface of a nanophotonic waveguide, and realize a chiral waveguide coupler in which the handedness of the incident light determines the propagation direction in the waveguide. We control the directionality of the scattering process and can direct up to 94% of the incoupled light into a given direction. Our approach allows for the control and manipulation of light in optical waveguides and new designs of optical sensors.

The development of integrated electronic circuits laid the foundations for the information age which fundamentally changed modern society. During the last decades, a transition from electronic to photonic information transfer took place and, nowadays, nanophotonic circuits and waveguides promise to partially replace their electronic counterparts and to enable radically new functionalities (*1*–*3*). The strong confinement of light provided by such waveguides leads to large intensity gradients on the wavelength scale. In this strongly non-paraxial regime, spin and orbital angular momentum of light are no longer independent physical quantities but are coupled (*4*, *5*). In particular, the spin depends on the position in the transverse plane and on the propagation direction of light in the waveguide—an effect referred to as spin-orbit interaction of light (SOI). This effect holds great promises for the investigation of a large range of physical phenomena such as the spin-Hall effect (*6*, *7*) and extraordinary momentum states (*8*), and has been observed for freely propagating light fields (*9*, *10*), in the case of total internal reflection (*11*, *12*), in plasmonic systems (*13*–*15*) and for radio frequency waves in metamaterials (*16*). Recently, it has been demonstrated in a cavity-quantum electrodynamics setup that SOI fundamentally modifies the coupling between a single atom and the resonator field (*17*).

For vacuum-clad dielectric waveguides, evanescent fields arise in the vicinity of the surface and allow one to locally interface the guided fields with micro- and nanoscopic emitters (*18*). Due to SOI, these evanescent fields exhibit a locally varying ellipticity which stems from a longitudinal polarization component that points in the direction of propagation of the light and that oscillates in quadrature with respect to the transversal components (*19*). Surprisingly and in contrast to paraxial light fields, the corresponding photon spin is in general not parallel or antiparallel to the propagation direction of the guided light. In special cases it can even be perpendicular to the propagation direction and antiparallel to the orbital angular momentum (*8*, *20*).

We experimentally demonstrate that SOI in a dielectric nanophotonic waveguide drastically changes the scattering characteristics of a nanoscale particle located in the waveguide's evanescent field. In free space, point-like scatterers exhibit a dipolar emission pattern (*21*) where, for the emission of both, linearly and circularly polarized light, the intensity distribution of the scattered light is cylindrically symmetric. In particular, this implies that dipolar scattering into any spatial direction perpendicular to the symmetry axis is always accompanied by an equal amount of scattered light into the opposite direction. We demonstrate that SOI breaks this symmetry, and show that when light is scattered by the particle into the waveguide modes, the amount of light that is coupled into a given direction of the waveguide can significantly exceed the power that propagates in the opposite direction.

We use an air-clad silica nanofiber as an optical waveguide and position a single spherical gold nanoparticle on its surface. We illuminate the particle with a focused paraxial laser beam from the side (Fig. 1A), and characterize the scattering properties of the particle into the optical waveguide. The emission rate of the particle into a given nanofiber eigenmode is proportional to $\left|\mathbf{d}^* \cdot \epsilon\right|^2$ with the induced electric dipole moment $\mathbf{d}$ of the particle and the profile function ϵ of the electric part of the fiber mode (*22*). For spherical scatterers, the dipole moment is $\mathbf{d} = \alpha \cdot \boldsymbol{\mathcal{E}}_{\mathrm{exc}}$, where α is the complex polarizability and $\boldsymbol{\mathcal{E}}_{\mathrm{exc}}$ is the positive frequency envelope of the excitation field which is related to the real value of the electric field by $\mathbf{E}_{\mathrm{exc}} = 1/2(\boldsymbol{\mathcal{E}}_{\mathrm{exc}}\exp(-i\omega t) + c.c.)$. Here, $\omega/2\pi$ is the frequency of the light and *c.c.* the complex conjugate. The total power of the light scattered into a given fiber mode is given by

$$I_{\mathrm{scat}} \propto \left|d^* \cdot \epsilon(r,\phi)\right|^2 = \left|\alpha^* \mathcal{E}_{\mathrm{exc}}{}^* \cdot \epsilon(r,\phi)\right|^2 \quad (1)$$

where (r, ϕ) denotes the position of the scatterer in the nanofiber transverse plane. As a consequence, the emission rate is directly proportional to the overlap between the field of the excitation light and the fiber mode at the particle's position.

For a single-mode nanofiber, all guided light fields can be decomposed into the quasi linearly polarized fiber eigenmodes (*19*), $HE^{\pm}_{11,x}$ and $HE^{\pm}_{11,y}$, where the *z*-axis coincides with the nanofiber axis and the ± sign indicates the propagation direction ($\pm z$) of the light in the fiber. We choose $HE^{\pm}_{11,x}$ and $HE^{\pm}_{11,y}$ such that their main polarization component points along x – ($\phi = 0°$) and y-direction ($\phi = 90°$), respectively. Figure 2 shows the normalized total power of the light scattered into the $HE^{\pm}_{11,x}$ - and $HE^{\pm}_{11,y}$ -modes, according to Eq. (1), as a function of the position of the scatterer in the fiber transverse plane. The calculations were performed for circularly $\sigma^{\pm} = i\mathbf{e}_z \pm \mathbf{e}_y/\sqrt{2}$ and linearly $\pi = \mathbf{e}_x$ polarized excitation light. Here, the *x*-axis is the quantization axis and $\mathbf{e}_{x,y,z}$ are the unit vectors along the corresponding axes. The predicted asymmetry of the scattering originates from the fact that the local polarization depends both on the position in the fiber transverse plane and on the propagation direction of the mode—a consequence of SOI of the nanofiber guided light. For a particle located at the top ($\phi = 90°$) of the nanofiber, the polarization overlap between the $HE^{+}_{11,y}$ ($HE^{-}_{11,y}$) mode and σ^- is maximal (minimal) and reaches 93% (7%), meaning that the field is nearly perfectly circularly polarized. Because the emission probability of the particle into the fiber is directly proportional to this overlap, a strong asymmetry of the scattering into the left (+*z*) and right (–*z*) direction of the fiber results, which can be tuned by the polarization of the incident

light field and the position of the nanoparticle. In particular, the asymmetry reverses when switching the polarization of the excitation light from σ^- to σ^+ or when changing the position of the particle from (x, y) to $(x, -y)$.

We investigate this directional scattering using a tapered optical fiber (TOF) with a nanofiber waist (*23*) (diameter: $2a = [315 \pm 3]$ nm) which enables almost lossless coupling of light from a standard optical fiber into and out of the nanofiber section. A single spherical gold nanoparticle (diameter: $2r = [90 \pm 3]$ nm) positioned on the nanofiber surface (*22*) acts as a polarization maintaining scatterer (*24*, *25*). The particle is illuminated with a laser beam propagating in the $-x$-direction (Fig. 1A) with a wavelength of 532 nm, close to the measured resonance of the nanoparticle at 530 nm (full width at half maximum: 50 nm). The nanofiber can be rotated around the *z*-axis, which, due to its cylindrical symmetry amounts to changing the azimuthal position ϕ of the nanoparticle around the fiber (Fig. 1A). The polarization of the incident light field is set by means of a quarter-wave plate. The angle θ between its optical axis and the *y*-axis can be adjusted at will. Before passing through the waveplate, the polarization of the light is aligned along *z*. Thus, we can set the polarization to linear along *z* ($\theta = 0°, 90°$) and circular, i.e., σ^- ($\theta = 45°$) or σ^+($\theta = 135°$). For intermediate angles the polarization is elliptical with the major axis along *z*. The excitation laser beam has a waist radius of around $w = 150$ μm at the position of the nanoparticle, thereby assuring a homogenous spatial intensity distribution with negligible longitudinal polarization components. A single photon counting module (SPCM) at each output port of the TOF detects the light scattered into the nanofiber. After completion of all measurements, we analyze the fiber surface with a scanning electron microscope (Fig. 1, C and D) to check that only a single nanoparticle was present and to measure the diameters of fiber and nanoparticle.

Figure 3 shows the measured photon fluxes at both fiber outputs (Fig. 3, A and B) as a function of the azimuthal position of the nanoparticle and the polarization of the excitation light field as well as the theoretical predictions (Fig. 3, C and D) calculated according to Eq. (1) under the assumption that the polarization and intensity distribution of the incident light field are not modified by the presence of the optical fiber (*22*). We find qualitative agreement between measurement and theoretical prediction. In particular, we observe the expected maximum of the left–right asymmetry for the case of circular input polarization with the particle located at the top or the bottom of the fiber. However, scattering and refraction of the excitation light field by the nanofiber lead to an appreciable modification of the polarization and intensity of the field close to the nanofiber surface, see Fig. 1B (*26*). Including these effects, we obtain the theoretical predictions shown in panels E and F, where we used two fit parameters: the angular offset $\phi_0 = 6.3° \pm 0.1°$ of the nanoparticle from the expected deposition position of $\phi = 90°$ and the amplitude $\kappa_f = (21.0 \pm 0.1) \times 10^6\ s^{-1}$ of the photon flux detected by the SPCMs (*22*). This model agrees well with the measured data. The main differences to the simple model are an increase of the scattering rate around $\phi = 180°$ due to the focusing of the incident light field by the fiber and the emergence of a shadow region around $\phi = 120°$ and $\phi = 240°$ with a concomitant decrease in the scattering rate.

For closer comparison, Fig. 4, A to D, shows the polarization dependence of the measured photon flux in the fiber for selected azimuthal positions of the nanoparticle together with the theoretical prediction. For the cases of the nanoparticle positioned near the top and the bottom of the nanofiber, we also plot the directionality

$$\mathcal{D} = \frac{c_+ - c_-}{c_+ + c_-} \quad (2)$$

of the scattering process together with the theoretical prediction (panels E and F), where, $c_+(c_-)$ is the photon flux detected by the left (right) detector. We observe a maximum directionality of $\mathcal{D} = 0.88$ ($\mathcal{D} = 0.95$) for a particle near the top (bottom) of the fiber which corresponds to a ratio of 16:1 (40:1) between the photon flux scattered to the left and right (right and left). When the particle is located near the side of the fiber, the overlap of the fiber eigenmodes with any polarization of the excitation light is independent of the propagation direction and zero directionality is expected. In the experiment, we indeed observe only a small variation with the incident polarization (Fig. 4, A and B). The residual modulation is most probably due to the small angular deviation of the nanoparticle position from the ideal point.

The underlying physical mechanism that enables the directional scattering is spin-orbit interaction of light which universally occurs in light fields that are strongly confined in the transversal direction. Our method is thus highly versatile and we expect it to find application in various scenarios of nanophotonic systems. Interestingly, there is no fundamental limit to the directionality: by setting the polarization of the excitation field orthogonal to the polarization of the fiber eigenmodes that copropagate into the left/right direction, unity directionality can always be realized (*22*). Moreover, at the inside of the waveguide, the quasi linearly polarized guided modes of our silica nanofiber exhibit a perfectly circular polarization at two specific positions in the fiber transverse plane. Thus, a particle at such a position that is excited with circularly polarized light will couple light exclusively into one direction of the waveguide. Apart from their usefulness for optical signal processing and routing of light, our findings have important consequences for the interaction between atoms and light in evanescent fields (*27*, *28*) or strongly focused laser beams. Moreover, they may enable novel nanophotonic sensors that allow one to detect and identify, e.g., scatterers with an intrinsic polarization asymmetry (*22*, *29*). In the course of preparing this manuscript we became aware of two related theoretical works (*30*, *31*) discussing effects based on directional emission in photonic crystal waveguides.

References and Notes

1. D. K. Gramotnev, S. I. Bozhevolnyi, Plasmonics beyond the diffraction limit. *Nat. Photonics* **4**, 83–91 (2010). doi:10.1038/nphoton.2009.282
2. O. Benson, Assembly of hybrid photonic architectures from nanophotonic constituents. *Nature* **480**, 193–199 (2011). Medline doi:10.1038/nature10610
3. L. Tong, F. Zi, X. Guo, J. Lou, Optical microfibers and nanofibers: A tutorial. *Opt. Commun.* **285**, 4641–4647 (2012) Special Issue: Optical micro/nanofibers: Challenges and Opportunities. doi:10.1016/j.optcom.2012.07.068
4. M. Onoda, S. Murakami, N. Nagaosa, Hall effect of light. *Phys. Rev. Lett.* **93**, 083901 (2004). Medline doi:10.1103/PhysRevLett.93.083901
5. A. David, M. Babiker, *The Angular Momentum of Light* (Cambridge Univ. Press, 2012).
6. K. Klitzing, G. Dorda, M. Pepper, New Method for High-Accuracy Determination of the Fine-Structure Constant Based on Quantized Hall Resistance. *Phys. Rev. Lett.* **45**, 494–497 (1980). doi:10.1103/PhysRevLett.45.494
7. S. Murakami, N. Nagaosa, S.-C. Zhang, Dissipationless quantum spin current at room temperature. *Science* **301**, 1348–1351 (2003). Medline doi:10.1126/science.1087128
8. K. Y. Bliokh, A. Y. Bekshaev, F. Nori, Extraordinary momentum and spin in evanescent waves. *Nat. Commun.* **5**, 3300 (2014). Medline doi:10.1038/ncomms4300
9. Y. Zhao, J. S. Edgar, G. D. M. Jeffries, D. McGloin, D. T. Chiu, Spin-to-orbital angular momentum conversion in a strongly focused optical beam. *Phys. Rev. Lett.* **99**, 073901 (2007). Medline doi:10.1103/PhysRevLett.99.073901
10. J. Korger, A. Aiello, V. Chille, P. Banzer, C. Wittmann, N. Lindlein, C. Marquardt, G. Leuchs, Observation of the geometric spin Hall effect of light. *Phys. Rev. Lett.* **112**, 113902 (2014). Medline doi:10.1103/PhysRevLett.112.113902
11. O. Hosten, P. Kwiat, Observation of the spin hall effect of light via weak measurements. *Science* **319**, 787–790 (2008). Medline doi:10.1126/science.1152697
12. K. Y. Bliokh, A. Niv, V. Kleiner, E. Hasman, Geometrodynamics of spinning light. *Nat. Photonics* **2**, 748–753 (2008). doi:10.1038/nphoton.2008.229

13. K. Y. Bliokh, Y. Gorodetski, V. Kleiner, E. Hasman, Coriolis effect in optics: Unified geometric phase and spin-Hall effect. *Phys. Rev. Lett.* **101**, 030404 (2008). Medline doi:10.1103/PhysRevLett.101.030404
14. F. J. Rodríguez-Fortuño, G. Marino, P. Ginzburg, D. O'Connor, A. Martínez, G. A. Wurtz, A. V. Zayats, Near-field interference for the unidirectional excitation of electromagnetic guided modes. *Science* **340**, 328–330 (2013). Medline doi:10.1126/science.1233739
15. J. Lin, J. P. Mueller, Q. Wang, G. Yuan, N. Antoniou, X. C. Yuan, F. Capasso, Polarization-controlled tunable directional coupling of surface plasmon polaritons. *Science* **340**, 331–334 (2013). Medline doi:10.1126/science.1233746
16. P. V. Kapitanova, P. Ginzburg, F. J. Rodríguez-Fortuño, D. S. Filonov, P. M. Voroshilov, P. A. Belov, A. N. Poddubny, Y. S. Kivshar, G. A. Wurtz, A. V. Zayats, Photonic spin Hall effect in hyperbolic metamaterials for polarization-controlled routing of subwavelength modes. *Nat. Commun.* **5**, 3226 (2014). Medline doi:10.1038/ncomms4226
17. C. Junge, D. O'Shea, J. Volz, A. Rauschenbeutel, Strong coupling between single atoms and nontransversal photons. *Phys. Rev. Lett.* **110**, 213604 (2013). Medline doi:10.1103/PhysRevLett.110.213604
18. M. J. Morrissey, K. Deasy, M. Frawley, R. Kumar, E. Prel, L. Russell, V. Truong, S. Nic Chormaic, Spectroscopy, Manipulation and Trapping of Neutral Atoms, Molecules, and Other Particles Using Optical Nanofibers: A Review. *Sensors (Basel Switzerland)* **13**, 10449–10481 (2013). doi:10.3390/s130810449
19. J. Fam Le Kien, Liang, K. Hakuta, V. Balykin. *Opt. Commun.* **242**, 445 (2004).
20. K. Y. Bliokh, F. Nori, Transverse spin of a surface polariton. *Phys. Rev. A* **85**, 061801 (2012). doi:10.1103/PhysRevA.85.061801
21. J. D. Jackson, *Classical Electrodynamics* (John Wiley & Sons, 1998).
22. Materials and methods are available as supplementary materials on *Science* Online.
23. G. Brambilla, Optical fibre nanowires and microwires: A review. *J. Opt.* **12**, 043001 (2010). doi:10.1088/2040-8978/12/4/043001
24. V. Myroshnychenko, J. Rodríguez-Fernández, I. Pastoriza-Santos, A. M. Funston, C. Novo, P. Mulvaney, L. M. Liz-Marzán, F. J. García de Abajo, Modelling the optical response of gold nanoparticles. *Chem. Soc. Rev.* **37**, 1792–1805 (2008). Medline doi:10.1039/b711486a
25. T. Bauer, S. Orlov, U. Peschel, P. Banzer, G. Leuchs, Nanointerferometric amplitude and phase reconstruction of tightly focused vector beams. *Nat. Photonics* **8**, 23–27 (2014). doi:10.1038/nphoton.2013.289
26. P. W. Barber, S. C. Hill, *Light Scattering by Particles: Computational Methods*, vol. 2 (World scientific, 1990).
27. E. Vetsch, D. Reitz, G. Sagué, R. Schmidt, S. T. Dawkins, A. Rauschenbeutel, Optical interface created by laser-cooled atoms trapped in the evanescent field surrounding an optical nanofiber. *Phys. Rev. Lett.* **104**, 203603 (2010). Medline doi:10.1103/PhysRevLett.104.203603
28. A. Goban, K. S. Choi, D. J. Alton, D. Ding, C. Lacroûte, M. Pototschnig, T. Thiele, N. P. Stern, H. J. Kimble, Demonstration of a state-insensitive, compensated nanofiber trap. *Phys. Rev. Lett.* **109**, 033603 (2012). Medline doi:10.1103/PhysRevLett.109.033603
29. R. Mitsch, C. Sayrin, B. Albrecht, P. Schneeweiss, A. Rauschenbeutel, arXiv:1406.0896 (2014).
30. A. B. Young *et al*., arXiv:1406.0714 (2014).
31. I. Söllner, S. Mahmoodian, A. Javadi, P. Lodahl, arXiv:1406.4295 (2014).
32. D. Axelrod, T. Burghardt, N. Thompson, Total Internal Reflection Fluorescence. *Annu. Rev. Biophys. Biol.* **13**, 247–268 (1984). doi:10.1146/annurev.bb.13.060184.001335
33. T. Kawalec, L. Józefowski, J. Fiutowski, M. Kasprowicz, T. Dohnalik, Spectroscopic measurements of the evanescent wave polarization state. *Opt. Commun.* **274**, 341–346 (2007). doi:10.1016/j.optcom.2007.02.042
34. V. I. Fam Le Kien, Balykin, K. Hakuta. *Phys. Rev. A* **73**, 013819 (2006).
35. S. J. Oldenburg, J. B. Jackson, S. L. Westcott, N. J. Halas, Infrared extinction properties of gold nanoshells. *Appl. Phys. Lett.* **75**, 2897 (1999). doi:10.1063/1.125183

Acknowledgements: We gratefully acknowledge financial support by the NanoSci-ERA network "NOIs" and the European Commission (IP SIQS, No. 600645). J.V. acknowledges support by the European Commission (Marie Curie IEF Grant 300392).

Supplementary Materials
www.sciencemag.org/content/science.1257671/DC1
Materials and Methods
Supplementary Text
References (*32*–*35*)

19 June 2014; accepted 26 August 2014
Published online 4 September 2014
10.1126/science.1257671

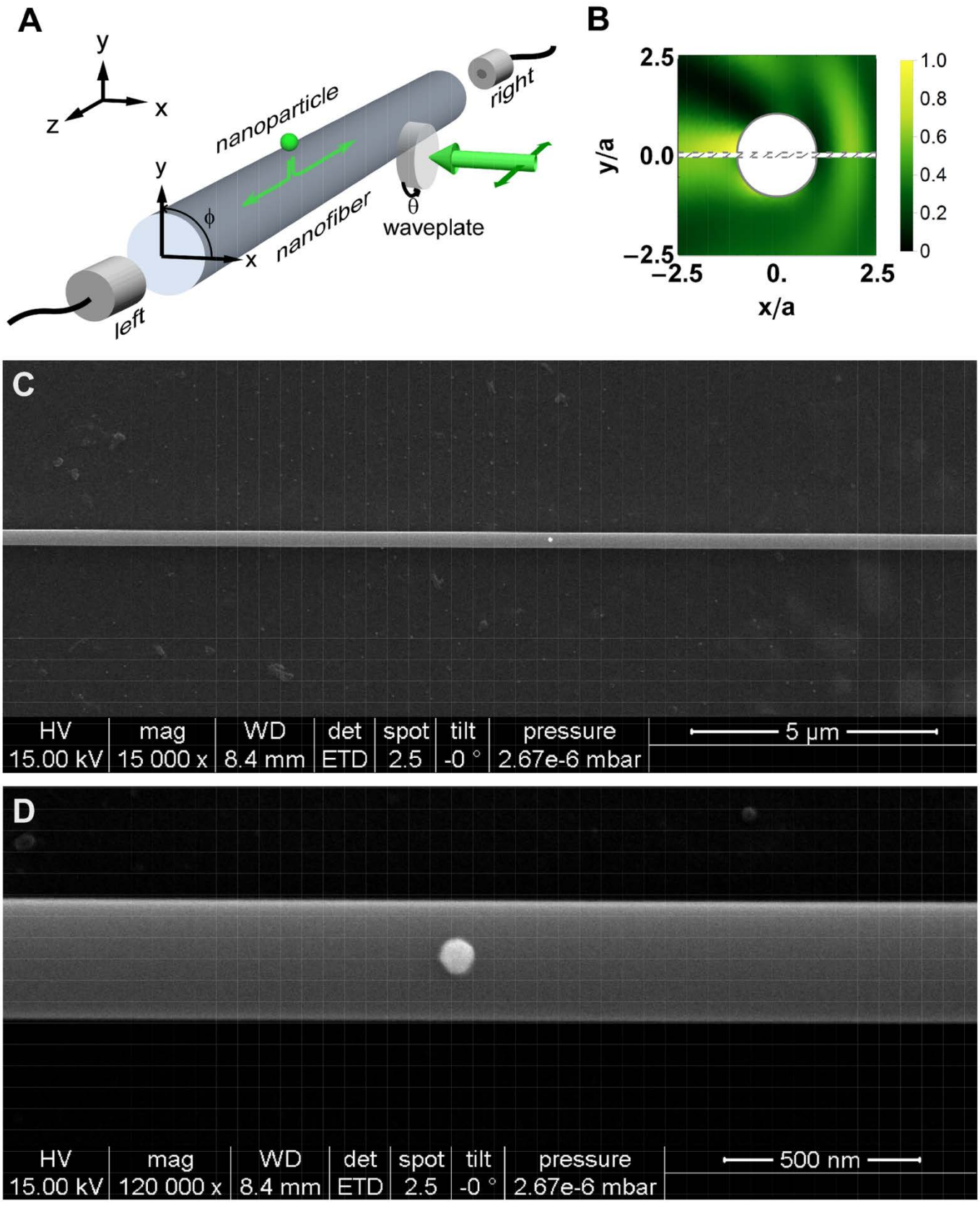
A
y
x
z
nanoparticle
right
y
ϕ
x
nanofiber
θ
waveplate
left
B
2.5
0.0
−2.5
y/a
−2.5
0.
2.5
x/a
1.0
0.8
0.6
0.4
0.2
0
C
HV
15.00 kV
mag
15 000 x
WD
8.4 mm
det
ETD
spot
2.5
tilt
-0 °
pressure
2.67e-6 mbar
5 µm
D
HV
15.00 kV
mag
120 000 x
WD
8.4 mm
det
ETD
spot
2.5
tilt
-0 °
pressure
2.67e-6 mbar
500 nm

Fig. 1. Experimental setup. (**A**) A single nanoparticle on a silica nanofiber surface is illuminated with light propagating in –*x*-direction. The polarization of the light can be set with a quarter-wave plate. The light scattered into the nanofiber is detected using single photon counting modules at the left and right fiber output port. (**B**) Modification of the intensity distributions for an incident field polarized along *y*- and *z*-axis due to the presence of the nanofiber. (**C** and **D**) Scanning electron microscope images of the nanofiber and the nanoparticle used in our experiments. From the images, we determine diameters of $2a = (315 \pm 3)$ nm for the fiber and $2r = (90 \pm 3)$ nm for the nanoparticle.

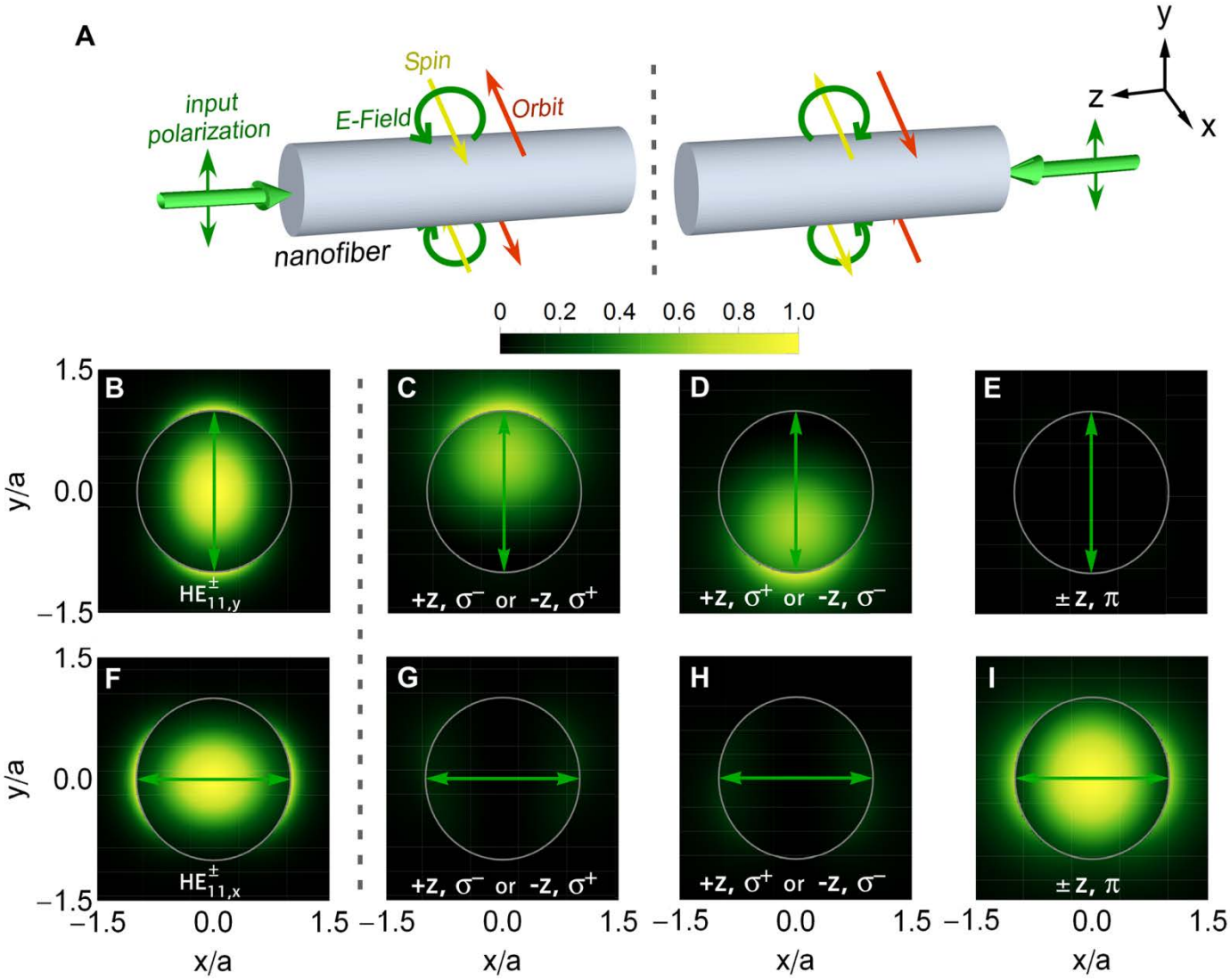

Fig. 2. Scattering in the presence of SOI (theoretical predictions). (**A**) When the nanofiber-guided light is quasi linearly polarized along the *y*-axis, longitudinal polarization components occur. For light traveling in +*z*-direction, this leads to nearly circular $\sigma^-(\sigma^+)$ polarization on the top (bottom) of the fiber, see circular green arrows. For light propagating in –*z* direction, $\sigma^- = \left(i\mathbf{e}_z - \mathbf{e}_y\right)/\sqrt{2}$ and $\sigma^+ = \left(i\mathbf{e}_z - \mathbf{e}_y\right)/\sqrt{2}$ are interchanged. At these positions, the spin angular momentum of the light (yellow arrows) is oriented perpendicular to the propagation direction and anti-parallel to the orbital angular momentum (red arrows), defined with respect to the *z* axis (*8*). (**B**) Intensity, $\left|\varepsilon^{\pm}_{HE,y}\right|^2$, of the $HE^{\pm}_{11,y}$ modes, normalized to its peak value on the fiber axis. (**C**) Position dependent power, scattered into the $HE^{+}_{11,y}$ ($HE^{-}_{11,y}$) mode for $\sigma^-(\sigma^+)$ polarized excitation light. (**D**) Power scattered into the $HE^{+}_{11,y}$ ($HE^{-}_{11,y}$) mode for $\sigma^-(\sigma^+)$ polarization. (**E**) Power scattered into the $HE^{\pm}_{11,y}$ modes for $\pi = \mathbf{e}_x$ polarization. (**F** to **I**) Same as B-E but for the fiber modes $HE^{\pm}_{11,x}$. The calculations assume our experimental parameters and the scattered powers are normalized to the peak value on the fiber axis in panel I. On top of the fiber ($x = 0$, $y = a$), we find a normalized power of 0.88, 0.06, and 0 in panels (C) to (E), respectively.

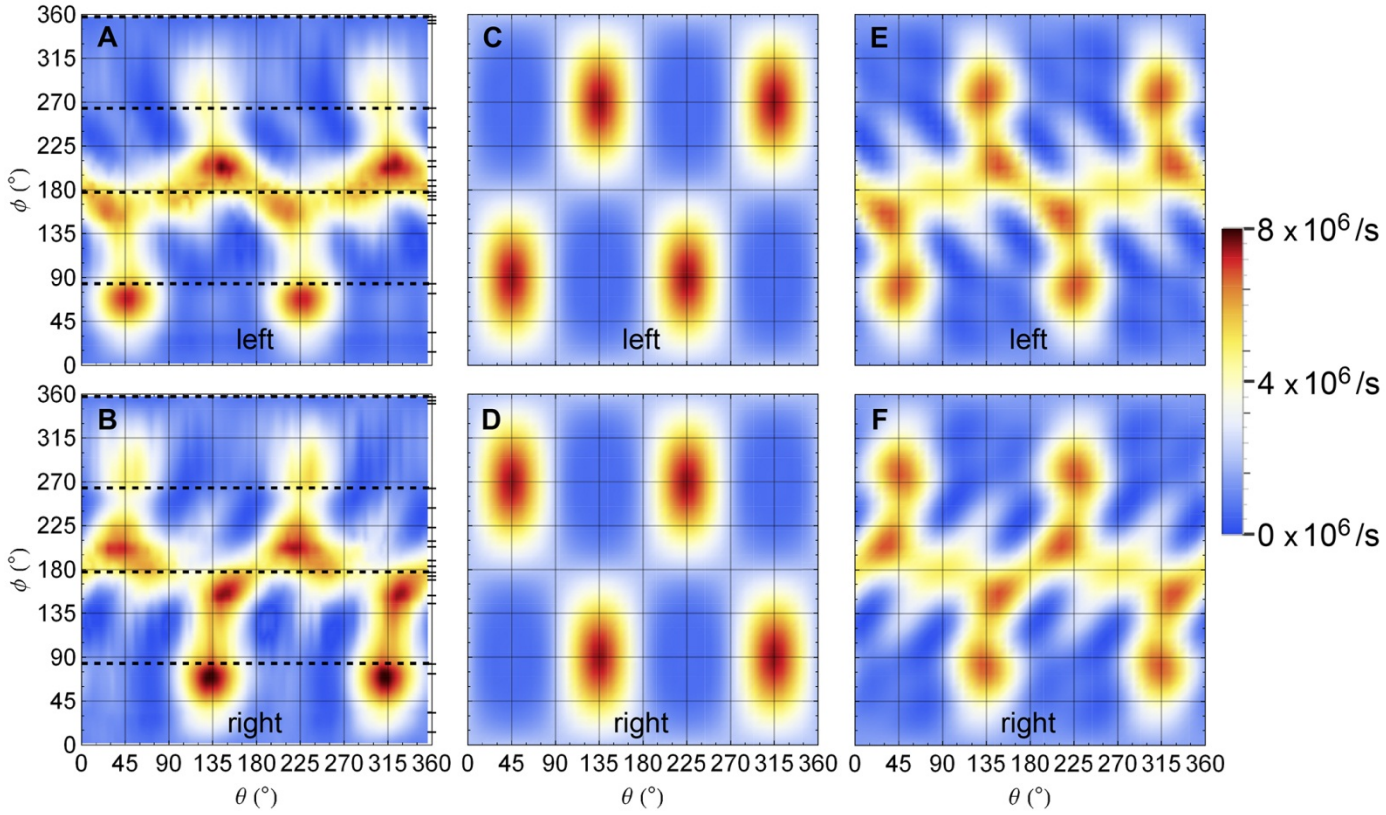

Fig. 3. Chiral waveguide coupling, experiment and theory. (**A** and **B**) Measured photon flux (raw data, only corrected for the nonlinear response of the SPCMs) of the light scattered into the left [right] direction as a function of the azimuthal position of the nanoparticle ϕ and the polarization of the excitation light field set by the angle θ of the quarter-wave plate. The ticks on the right side of the panels mark the azimuthal positions for which data has been acquired with a stepsize of θ of 5°. The data are interpolated in between the measured points. The dashed lines indicate the datasets plotted in Fig. 4. (**C** to **F**) Theoretical prediction for the photon fluxes when neglecting [including] the effect of the nanofiber on the incident light field. The model uses the angular offset of the nanoparticle and the overall amplitude of the photon flux as free parameters which are obtained from a fit of (E) and (F) to the data in (A) and (B) (*22*).

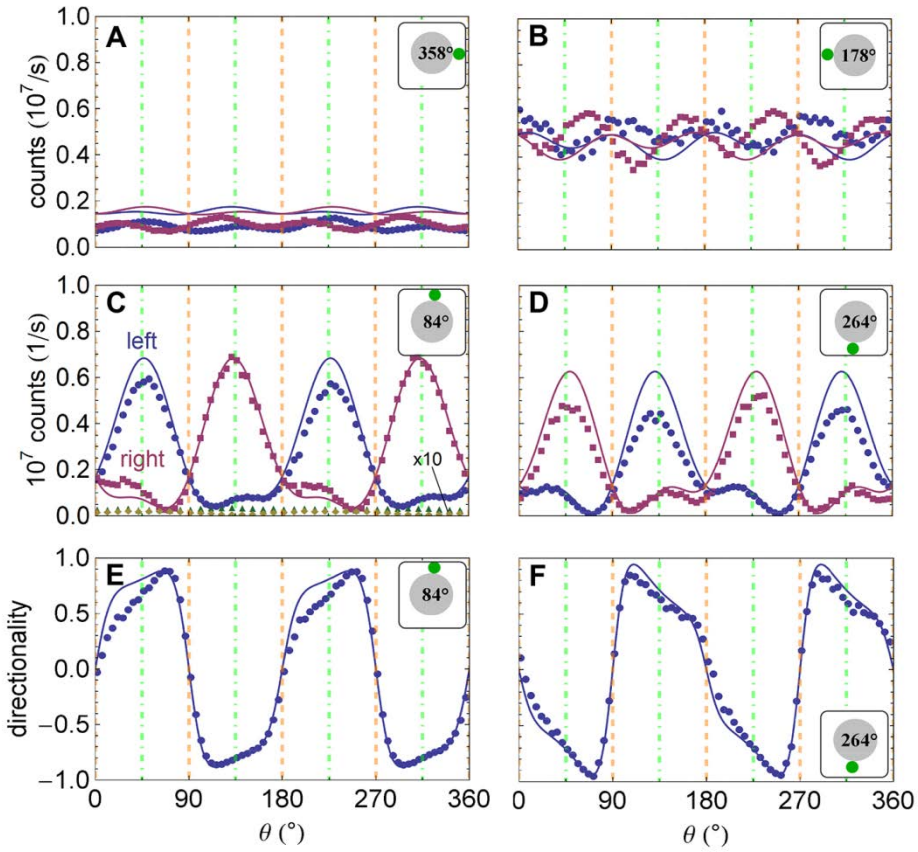

Fig. 4. Directionality of the scattering process. (**A** to **D**) Measured photon fluxes at the left (blue circles) and right (red squares) fiber output port as a function of the angle θ of the quarter-wave plate. Here, θ = 0, 90, ... corresponds to linear polarization along z (dashed orange lines) and θ = 45, 225 (θ = 135,315) corresponds to $\sigma^-(\sigma^+)$ polarization of the incident light field (dash-dotted green lines). (A) to (D) correspond to the azimuthal positions (ϕ = 358, 178, 84, and 264) of the nanoparticle (green dot) around the fiber (gray disk), as indicated in the insets. The solid lines are the predictions of our theoretical model. The statistical error bars are too small to be visible in the plot. (C) also shows exemplarily the measured photon fluxes to the left (yellow diamonds) and right (green triangles) for the nanofiber without the nanoparticle, scaled up by a factor of 10. (**E** and **F**) Directionality $\mathcal{D}$ of the scattering process into the fiber for the data in (C) and (D).